Compact Modeling and Contact Effects in Thin Film Transistors

Juan Antonio Jiménez Tejada, *Member, IEEE*, Juan Antonio López Villanueva, *Senior Member, IEEE*, Pilar López Varo, *Member, IEEE*, Karam M. Awawdeh, and M. Jamal Deen, *Fellow, IEEE*

(*Invited Paper*)

***Abstract*— A compact model for the current–voltage characteristics of organic thin-film transistors (OTFTs), which includes the effects of the contact regions, is proposed. Different physical and morphological aspects of contacts with organic or other emerging materials such as graphene, semiconducting dichalcogenides such as MoS_2, or NW devices are described. The electrical behavior of the contacts is studied in OTFTs, and circuit models that describe them are reviewed. Two trends are observed in the current-voltage curves of the contacts of different OTFTs: linear and nonlinear, and different models are used to explain them. A unified model for the contact region that reproduces both trends and gathers the different physical and structural features of the contacts is developed. It is described by a single parameter and introduced in a generic analytical model for TFTs. The variability in OTFT structures, materials, and fabrication approaches gives rise to a strong variability in the values of the parameters of the model. In this regard, a characterization technique to determine the value of the parameters of the model from experimental data is also developed. Different physical tests are proposed to validate the results of the technique. The procedure is applied to recent experimental data for different pentacene-based transistors. The good agreement between the experimental data and our analytical results provides a way to relate the parameters of the model with the physical or geometrical origin of the contact effects in OTFTs.**

***Index Terms*— Compact modeling, contact effects, contact modeling, organic thin-film transistor (OTFT), organic transistors, OTFT modeling, thin film transistors (TFTs).**

I. Introduction

EMERGING technologies based on organic or polymeric materials [1]–[3], 2-D materials such as graphene [4], semiconducting dichalcogenides, MoS_2 or WSe_2 [5], or nanowire (NW) devices [6], are promising solutions in the fields of nanoelectronics, sensing, and photonics. Apart from having common applications, these materials share an additional common feature: the connection to the outer world via metal contacts.

In order to treat this common contact problem, we focus on one of these emerging technologies and one of its outstanding devices, the organic or polymeric (hereafter, the term organic is used for both) thin-film transistor (OTFT). These transistors are especially important as drive elements in niche applications such as the displays of mobile devices and televisions using the Active-Matrix Organic Light-Emitting Diode technology. Sensors, smart labels, solar cells, or smart clothing are other emerging and innovative applications where these transistors work as the main or control element. These transistors, and other organic devices, have received considerable attention because of the attractive properties of the materials they use. One key advantage of the organic material is that they can be solution processed [7]. The combination of soluble deposition techniques such as drop casting, spin coating, layer-by-layer, or roll-to-roll on flexible sheets with low-cost patterning equipment, such as ink-jet printers [8], reduces both capital and manufacturing costs compared with conventional crystalline electronics [9].

Contact effects in OTFTs are affected by the materials used for substrates, electrodes, or semiconducting films; the vertical and horizontal layout differences; the different processing steps such as vacuum processing, spin coating, printing, or stamping; the functionalization of interfaces; and the self assembling of organic materials. Though important in all devices, the contact effects are even stronger at the nanoscale [10]. To understand the effects of the contacts in OTFTs, the physical or geometrical origins of these effects are treated jointly in nanoscale and organic-thin-film structures.

The prediction and optimization of the performance of integrated circuits is necessary. For practical applications, compact models for electronic devices play an important role. Compact models must include the effects of beneficial and detrimental mechanisms that affect the device performance. In this paper, we focus on the incorporation of the contact effects in compact models of OTFTs.

This paper begins with the analysis of the properties of the contacts from a general point of view, treating common effects at nano- and large scale (Section II). In Section III, we analyze the advantages and disadvantages of previously developed models that describe the current–voltage curves of OTFTs with contact effects. In Section IV, we propose a compact model for the contact region of OTFTs that unifies different

Manuscript received June 29, 2013; revised August 25, 2013; accepted September 18, 2013. Date of publication January 2, 2014; date of current version January 20, 2014. This work was supported in part by the Ministerio de Educación y Ciencia and in part by the Fondo Europeo de Desarrollo Regional under research Project TEC2010-16211. The work of M. J. Deen was supported by the Canada Research Chair program. The review of this paper was arranged by Editor B. Iñiguez.

J. A. J. Tejada, J. A. L. Villanueva, P. L. Varo, and K. M. Awawdeh are with the Departamento de Electrónica y Tecnología de los Computadores, Universidad de Granada, Granada 18071, Spain (e-mail: tejada@ugr.es; pilarlopez@ugr.es; jalopez@ugr.es; karamawawdeh17@yahoo.com).

M. J. Deen is with the Department of Electrical and Computer Engineering, McMaster University, Hamilton, ON L8S 4K1, Canada (e-mail: jamal@mcmaster.ca).

Digital Object Identifier 10.1109/TED.2013.2282994

0018-9383 © 2014 IEEE. Personal use is permitted, but republication/redistribution requires IEEE permission.
See http://www.ieee.org/publications_standards/publications/rights/index.html for more information.

trends found in the literature. This model is introduced in Section V in a previously developed generic model for OTFTs. In the following sections, the resulting model is applied to describe recent experimental data in OTFTs with contact effects.

II. Properties of Metal Contacts

Although the basic ideas of the metal-semiconductor contacts are reasonably well understood [11], [12], there are many side effects that impact their electrical behavior (Fig. 1). Here, we analyze the role of metal contacts in general terms, distinguishing between physical and geometrical effects.

A. Metal and Semiconductor Work Functions

According to the earliest and simplest models of the metal-semiconductor junction [13], [14], the difference between the metal and semiconductor work functions determines the ohmic or rectifying behavior of the contact. As an example, in graphene, Pd and Ni have been shown to provide a relatively low contact resistance. A higher contact resistance has been observed with Ti, Cr, and Al contacts [15]–[17].

The doping level in the semiconductor, even in bulk metal-semiconductor junctions, determines the position of the Fermi level in relation to the band edges, and thus the semiconductor work-function. Graphene displays an even stronger effect known as metal doping. Since monolayer graphene is gapless, realignment of the Fermi level due to the metal work function and the accompanying charge transfer can produce p-type or n-type behavior. In fact, a very small amount of electron transfer shifts the Fermi level significantly in graphene [18]. Thus, contacts in graphene can be chosen as n-type or p-type by selecting a metal with the suitable work function. When the graphene layer is deposited on a bottom gate, separated from it by a thin insulator layer, and then covered by a top contact (TC), the bottom gate bias has also been found to contribute to the metal-graphene contact resistance by changing the charge density in the graphene layer [15], [16].

B. Quality of the Contact and the Near-Interfacial Region

The position of the Fermi level is also affected by the bond structure of the contact region, with possible bond polarization [19] and/or a high interface state density in the semiconductor gap [20], [21]. A charge neutrality level is defined at the position of the Fermi level at the interface for which the net charge in the interface states is zero. The Fermi level is said to be pinned [22], [23]. It cannot shift very much from this position without a huge charge transfer. Thus, the resulting barrier height may be significantly different from that predicted by using the work functions of the separate materials. There are approaches to de-pin the Fermi-level and tune the metal-organic contact behavior such as the introduction of ultrathin interfacial insulators (Si_3N_4) [24]; the treatment of the contacts with a self-assembled monolayer (SAM) [25]; the introduction of a thin polyelectrolyte layer between the electrodes and the semiconductor [26]; or using a solid electrolyte directly as dielectric layer [27]. These observed reductions in the contact

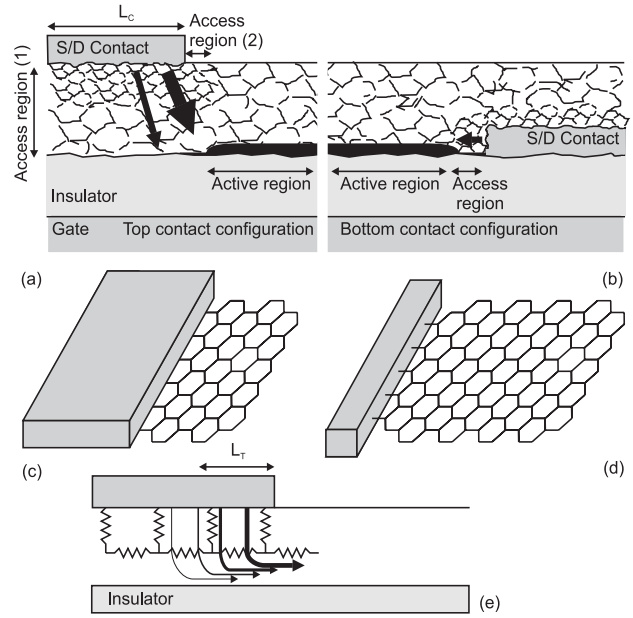

Fig. 1. Bottom-gate (a) staggered and (b) coplanar configurations showing side effects that determine the electrical behavior of a metal-semiconductor structure. (c) Side contact. (d) End or edge contact. (e) Current crowding.

resistance can be explained either by a decrease of the barrier energy or by changes in the surface morphology [25].

Examples of this last effect can also be seen in different materials as graphene, MoS_2, or NWs. Graphene can be subjected to strong modifications originated by charge inhomogeneities induced by the metal [28], [29]. Questions have arisen as to whether the original work function of the graphene is preserved after the contact [17]. Density functional theory calculations have shown that the energetic separation between the Fermi level and the Dirac point in the contacts is a sensitive function of the metal-graphene distance [18]. In [28], it was found that the metal-graphene coupling strength is moderate, resulting in a modification of the graphene density of states (DOS) underneath the contacts small enough so that Fermi level pinning does not occur due to a lack of screening of the gate field. Furthermore, although capacitance-voltage measurements have shown that the original work function of graphene is not preserved, but it is pinned to the work function of the metal when the coupling is strong, the measurement of the quantum capacitance of graphene in the strong accumulation mode seems to prove that the characteristic properties of the graphene DOS are maintained [17].

A further difference in behavior of graphene contacts has been proposed to distinguish between side-bonded [Fig. 1(c)] and end- or edge-bonded [Fig. 1(d)] contacts [30]. While end contacts form strong covalent bonds to the dangling bonds at the edges, top, and bottom contacts (BC) form weaker van der Waals bonds. In both cases, results show that Fermi-level pinning has a small influence in the barrier height, in contrast with what happens in bulk metal-semiconductor junctions.

In the case of contacts to layered MoS_2, the widely used Au contact has been proposed to form a tunnel barrier and be the cause of the low values of the measured mobility [5], while metals with a low work function would efficiently

inject electrons into the conduction band and would solve this problem. MoS_2 transistors with Sc [31] and Ti ohmic contacts [32] have been demonstrated, but the quality of the contacts should be improved in order to achieve the expected advantages of these materials.

While metal-induced gap states often determine the barrier height in bulk contacts, they can have a weaker impact in NWs. The electrostatics at reduced dimensions prevents the Fermi-level from being pinned since a strong band bending cannot be established due to the small size of these nanostructures. The region of a NW under the metal has also been shown to change its electrical properties after the application of a thermal treatment [6], [33].

In the case of OTFTs, the quality of the contacts also depends on the relative position of the source/drain (S/D) contacts, dielectric, and organic films. Bottom-gate OTFTs can be found in two typical structures: TC or staggered configuration [Fig. 1(a)] and BC or coplanar configuration [Fig. 1(b)]. The BC configuration is known to give inferior performance to the TC configuration for a range of deposition conditions and material thickness [34]. This can be attributed to the different arrangement of molecules in the organic material in relation to the proximity with other materials [34], [35].

C. Geometry of the Contact

The size and geometry of the electrodes are other factors that affect the performance of the transistors [36]. The description of the current flow through the contact region often requires a 2-D analysis, in particular for the TC staggered configuration [37], since the electrodes, dielectric, and semiconductor channel are not adjacent to each other [Fig. 1(e)]. A widely used model to deal with these aspects is the transmission-line (or transfer length) model (TLM) [38]. According to this model, instead of the physical length L, a contact transfer length, L_T, can be defined as the effective length over which injection occurs from the contact edge. In contacts to bulk and thin-film materials, $L_T = \sqrt{\rho_c/R_s}$, where ρ_c is the contact resistivity and R_s is the sheet resistance under the contact. The transfer length determines the contact resistance through the relation $R_c = \sqrt{\rho_c R_s}\tanh^{-1}(L/L_T)/w$ [38], [39], where w is the width of the contact.

The conventional expression of the TLM model has been applied to graphene [40]. To compute the transfer length in this system, a phenomenological expression for the sheet resistance of graphene under the contact [41] has to be used. This sheet resistance underneath the metal contact depends on the mobility, which in turn is strongly dependent on the deposition processes [10]. Experimental values of the contact transfer length in graphene show a dependence with the type of electrode [38]. The dependence on the material can be explained by the strength of the coupling between the metal and the semiconductor, since stronger coupling produces higher electron scattering and thus smaller L_T values. The TLM has also been applied to NWs [42]. However, corrections are introduced due to the small dimensions of these structures: the contact length in many NW devices is typically comparable to the NW length; and the depth of the depleted or accumulated semiconducting region in metal-NW interfaces is typically comparable to the NW radii [43].

D. Transition Region

The region within the semiconductor in which the effects of the contact are still strong is called the transition or access region [Fig. 1(a) and (b)]. The band bending due to the contact can be extended on a length scale of tens of nanometers to micrometers. This region, called depletion layer in bulk junctions, develops beneath the contact, but it can spread out laterally toward the channel in thin films and nanostructures. If the thickness of the depletion layer, W, is greater than the film thickness or the radii of the nanostructure, then W becomes size dependent and increases strongly at low doping concentrations. A long-distance band bending has been observed in NWs [44] and graphene [45]. A correct determination of W is important since its value strongly influences the charge-injection in the contact [46]. As in bulk contacts, a heavy doping can be used in end-bonded NWs to reduce W, thus allowing electrons to tunnel though the barrier. Nevertheless, this method cannot be used in the case of side contacts since, for this to be useful, W has to be smaller than the section diameter and a high doping level should be required when the NW diameter is reduced [46].

The change in the work function of graphene under metal also leads to band bending from the contact edge toward the channel [45], [47]. In the application of the TLM model to graphene, the contact resistance has been separated into two components: the actual contact resistance at the metal-graphene contact, R_{CI}, and the additional resistance due to the metal-contact doping, R_{CD} [40]. This component, R_{CD}, arises in the transition region along which the Fermi level varies from the value pinned by the metal due to metal doping to the value in the channel region. Thus, it depends on the type of metal and differs significantly for each metal. The very small DOS around the Fermi level for graphene increases the screening length. The resulting long charge transfer region is a unique characteristic of the metal/graphene contact [10] and was reported to be $\simeq 0.5$ μm [47].

In the transition region of the contacts of OTFTs, another mechanism takes place. The charges that are created near the surface of the electrode move through the organic material due to the electric field and the charge transport is space-charge limited. In the following sections, we discuss contact effects in TFTs.

III. Contact Effects in OTFTs

A. Models of Contact Effects

The objective, when modeling the contacts of OTFTs, is the reproduction of the current–voltage curves in the contact (I_D–V_C), where V_C is the voltage drop in the contact region, and their dependences on bias voltages, temperature, and material parameters [48], [49]. The incorporation of physical models of the contacts, [11], [50], into the classical transistor models is not a trivial task because the contact effects interfere with other dependences in OTFTs [1]. In the literature, there are different electrical models that incorporate the voltage drop

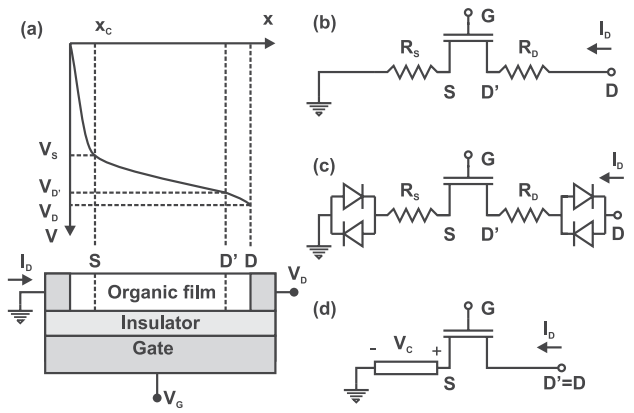

Fig. 2. (a) Separation of the channel of an OTFT in the active channel and the contact regions. Equivalent circuits of an OTFT including (b) linear source and drain contact resistances, (c) nonlinear model for the source and drain contact regions [51], and (d) our unified I_D–V_C model for the source contact assuming a negligible voltage drop at the drain contact [48].

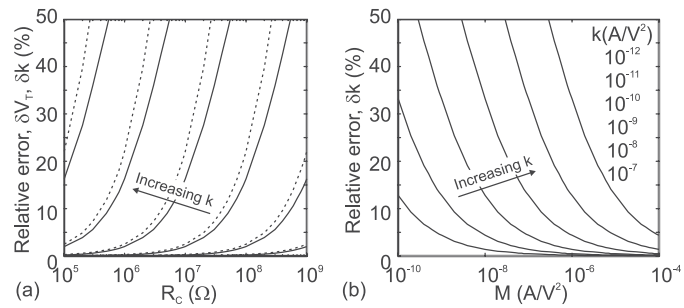

Fig. 3. Relative error in the determination with the ideal MOS model of the transconductance FET parameter, δk (solid lines) and the threshold voltage δV_T (dashed lines) in an OTFT with contact effects. The error is evaluated as a function of the contact related parameters (a) R_C and (b) M for different values of the transistor transconductance parameter k.

at the contacts [Fig. 2(a)]. There are also associated methods to extract this voltage drop from the output characteristics of a transistor [2], [51]–[55].

The low conductivity region close to the contact is usually modeled with a parasitic resistance R_C [Fig. 2(b)]. Experimental investigations show that the magnitude of R_C is dependent on the gate bias, temperature, and ambient gas environment [2], [36], [52], [56].

Nonlinear behavior, also observed in the literature, are treated with a drain-voltage-dependent resistance [53], [54]. The slope of the I_D–V_C curve increases with V_D, thus decreasing the contact resistance, being negligible in the saturation region [57]. This may be one reason for some authors to extract the field-effect mobility from the saturation region using the ideal MOS model [53], [58], [59]. However, this way to model nonlinear behavior can lead to confusion as noted in [60], where a diode was added in series with the contact resistance to model the nonlinear response. A study of the error made in the extracted values of the threshold voltage and mobility when considering the ideal MOS model in saturation is given in Section VI-A and Fig. 3. Better approaches that considers highly nonlinear drain and source contact series resistances and a gate-voltage-dependant mobility, ($\mu \propto (V_G - V_T)^{\gamma}, \gamma > 0$), can be found in the literature [51], [60]–[62]. This mobility dependence is extracted from theories such as the charge drift in the presence of tail-distributed traps (TDTs) [63] or variable range hopping (VRH) [64], [65]. In order to simulate nonlinear I_D–V_D output characteristics for organic BC TFTs, an equivalent BC TFT circuit that consists of the TFT with linear source and drain access resistances R_D and R_S, respectively, and a pair of anti-parallel leaky Schottky diodes connected to each access resistor in series, see Fig. 2(c), was proposed [51]. Two diodes in parallel are needed to obtain symmetric current–voltage characteristics. The diode nonideality factor, η, which is responsible for the steepness of the current–voltage characteristic, and the access resistances are the fitting parameters [51].

Recently, Schottky barriers at both drain and source contacts and electric field-dependent mobilities have been incorporated in 2-D numerical simulations to provide a vision on how the current spreads over the contact electrode [66], [67]. Although this model reproduces experimental data, the authors noted the sub-optimal values of some of the model parameters, such as the barrier height [67] or the diode nonideality factor, η [51]. Our interpretation is that simple electrical models valid for crystalline structures are substituting the two main physical theories that describe the metal-organic structure, injection, and space-charge-limited theories, thus providing suboptimal values for the model parameters.

B. What is Missing?

Linear or nonlinear contact behaviors are observed experimentally at low-drain voltages in the output characteristics of the transistor. Different physical mechanisms have been proposed to explain such behavior [68], [69]. However, many of the models used to interpret the effect of the contacts on these I–V curves are reduced to finding a value for the contact resistance.

A suitable OTFT model should incorporate both linear and nonlinear behaviors for the contact I–V curves, with a method that unifies in some of its parameters the injection and transport mechanisms present in the metal-organic contacts and that considers the dependence of the I–V curves with the gate voltage and the temperature. In the following sections, we present such a model.

Also needed is a method that can be used to extract, from the I–V experimental data of a single transistor, [70] the parameters of the transistor, including those associated with the contact region. Many methods to extract the parasitic resistance are based on a set of transistors with different lengths, or on more complex techniques such as the four-probe method or the sophisticated electrical scanning probe microscopy techniques [71]–[73]. In this paper, we combine the proposal of a compact model for OTFTs including contact effects with a method to extract I–V curves at the contact from output characteristics measured in a single transistor.

IV. Compact Model for the Contact Region of OTFTs

Different physical ways to inject charge from the metal contact (ohmic contacts, Schottky barriers, tunnel injection)

give way to linear or nonlinear contact behavior. Our method unifies all these physical mechanisms and behaviors by considering them as part of the boundary value for the charge density at the metal-organic interface, $qp(0)$. Its value must contain information about the physical, morphological, and/or geometrical features of the contact region. Some of the charges get trapped, with no contribution to the current. The rest, the free-charge density $q\theta p(0)$, where θ is the ratio of free to total charge density, drifts through localized sites in the transition region of the contact, as mentioned at the end of Section II. Independent of the value of $p(0)$, or how this charge has appeared at the metal organic interface, a relation between the current density j and the applied voltage V_C can be found by solving the transport equations in the semiconductor [55], [68]

$$V_C = (2/3)\,[2j/(\varepsilon\mu\theta)]^{1/2}\left[(x_C + x_p)^{3/2} - (x_p)^{3/2}\right]$$
$$x_p \equiv j\varepsilon\theta/\left\{2\mu\,[\theta qp(0)]^2\right\} \quad (1)$$

where $j = I_D/S$, S is the cross section of the channel where current I_D flows, x_p is a characteristic length defined as the point from the contact interface toward the organic film, at which the charge density $qp(x_p)$ decays to $qp(0)/\sqrt{2}$, ε is the organic dielectric constant, and x_C is the length of the contact region in the organic material, which may include the transition layer defined in Section II. Equation (1) was demonstrated to have two asymptotic trends: a linear or Ohmic behavior if the characteristic length x_p is a few times larger than the contact length x_C

$$I_D \approx S\theta \mathrm{qp}(0)\mu V_C/x_C \equiv V_C/R_C \quad (2)$$

and a quadratic behavior (Mott–Gurney law) if the characteristic length x_p is much smaller than the contact length x_C [55], [74]

$$I_D \approx \frac{9}{8}\varepsilon\mu\theta S V_C^2/x_C^3 \equiv M V_C^2. \quad (3)$$

The two asymptotic situations defined in (2) and (3) also define limit distributions of the free charge density in the contact, $\mathrm{qp}_{\mathrm{contact}}$. In the case of linear characteristics, $\mathrm{qp}_{\mathrm{contact}}$ is constant and its value can be represented by the value this variable takes at $x = 0$, $\mathrm{qp}_{\mathrm{contact}} = \theta qp(0)$, which is the value that appears in (2). The effective area of the contact where the current flows can be expressed as $S = w \times t_C$, where t_C is an effective thickness, and w is the contact width. Considering the free-charge surface density $\sigma_{\mathrm{contact}} = \theta \mathrm{qp}(0) t_C$, the following relation is obtained from (2):

$$\sigma_{\mathrm{contact}} = x_C/(w\mu R_C). \quad (4)$$

In the case of quadratic behavior, the distribution of the free charge density, not uniform along the contact region [50], is given by

$$\mathrm{qp}_{\mathrm{contact}}(x) = [(j\varepsilon\theta)/(2\mu x)]^{1/2}. \quad (5)$$

If the parameter M is known (in Section VI, a parameter extraction method is proposed), p_{contact} can be evaluated as a function of arbitrary values of the contact voltage V_{C_0} and the position x_0 close to the contact. This provides physical information about the extracted parameter M. In order not to work with the unknown effective thickness t_C, the free charge surface density is evaluated instead, $\sigma_{\mathrm{contact}} = \mathrm{qp}_{\mathrm{contact}}(x_0) \times t_C$. Thus, combining (3), (5) and $j = M \times V_{C_0}^2/S$, the following relation results:

$$\sigma_{\mathrm{contact}}(x_0) = (2MV_{C_0})/(3\mu)\left[(x_C^3)/(x_0 w^2)\right]^{(1/2)}. \quad (6)$$

The inverse of the contact resistance R_C in (4), and the parameter M in (6) are proportional to the free-charge surface-density $\sigma_{\mathrm{contact}}$. Thus, whatever trend $\sigma_{\mathrm{contact}}$ has with the gate voltage, the parameters $1/R_C$ and M will have the same trend, except for a multiplying factor.

V. Incorporation in an OTFT Model

The model for the contact region presented above is useful when integrated in a compact model for OTFTs. For this reason, we consider a generic analytical model for the current–voltage characteristics of OTFTs [61], [62]. In that work, the authors related the drain current I_D and the voltages at the borders of the intrinsic transistor, V_G, V_D, and V_S [Fig. 2(c)]

$$\frac{I_D}{k_o} = \frac{[(V_G - V_T - V_S)^{\gamma+2} - (V_G - V_T - V_D)^{\gamma+2}]}{\gamma + 2}$$
$$k_o = \mu_o C_i w/L \quad (7)$$

where $C_i = \varepsilon_i/t_i$ is the gate insulator capacitance per unit area, ε_i is the insulator dielectric constant, t_i is the insulator thickness, V_T is the threshold voltage, w is the transistor width, and L the channel length. The result is equivalent to the well-known and widely used generic FET model with a constant mobility. This model is derived considering that the voltage drop at the drain contact is small in comparison to the voltage drop at the source contact [48] [Fig. 2(a)]. Thus, the contact voltage is reduced to the voltage drop between the external source terminal and the internal source ($V_S \equiv V_C$) [Fig. 2(d)]. It also considers that the mobility μ is written according to the aforementioned common theoretical result [63], [64], [75]

$$\mu = \mu_o(V_G - V_T - V_x)^{\gamma}, \qquad \gamma = 2T_o/T - 2 \quad (8)$$

where V_x is the potential in the semiconducting film of the TFT, γ is the mobility enhancement factor, T_o is the specific equivalent temperature that represents the steepness of the DOS exponential tail, and μ_o is the mobility-related parameter with dimensions $\mathrm{cm}^2/(\mathrm{V}^{1+\gamma}\,\mathrm{s})$. In order to provide a single value for the voltage dependent mobility, the mobility is evaluated at $V_{GT} = V_G - V_T = 1$ V [61], thus $\mu(V_{GT} = 1\ \mathrm{V}) = \mu_o$ in $\mathrm{cm}^2/(\mathrm{Vs})$.

This model (7) is complemented with a model for the current–voltage curves in the contacts, as defined in (2) or (3). A new parameter, R_C (or M), not present in (7), is added to the set of parameters of the model. The parameters R_C and M are expected to depend on the gate voltage, as many experiments have shown the dependence of the I–V curve at the contacts with the gate voltage [2], [52], [76].

To describe this dependence, we analyze the two regions of different conductivity distinguished along the channel of the organic transistor [3], [48], [77]: the low conductivity region close to the contact defined by the free-charge surface-density $\sigma_{\mathrm{contact}}$ and the high conductivity region in the intrinsic

channel defined by its counterpart free-charge surface-density, usually expressed as [78]

$$\sigma_{\text{channel}} = C_{\text{i}}(V_{\text{G}} - V_{\text{T}}). \tag{9}$$

The free charge density in the contact region can be considered as a fraction of the last one: $\sigma_{\text{contact}} = \sigma_{\text{channel}}/K$. Although K is an undetermined constant, there is no physical reason to believe that the mobile charges in these two adjacent regions start appearing at very different gate voltages, or follow very different trends, unless local nonuniformities were present just at the contact region. Therefore, σ_{contact} can be assumed proportional to $(V_{\text{G}} - V_{\text{T}})$. Introducing this dependence and the gate voltage dependence of the mobility (8) in (4) and (6), we can write, respectively

$$1/R_{\text{C}} = [(wC_{\text{i}}\mu_{\text{o}})/(Kx_{\text{C}})](V_{\text{G}} - V_{\text{T}})^{(1+\gamma)} \tag{10}$$
$$M = \frac{3C_{\text{i}}\mu_{\text{o}}}{2KV_{\text{C}_0}}\left[\frac{x_0 w^2}{x_{\text{C}}^3}\right]^{1/2}(V_{\text{G}} - V_{\text{T}})^{(1+\gamma)}$$

or by defining the parameters α_1 and α_2

$$1/R_{\text{C}} = \alpha_1(V_{\text{G}} - V_{\text{T}})^{(1+\gamma)} \tag{11}$$
$$M = \alpha_2(V_{\text{G}} - V_{\text{T}})^{(1+\gamma)}.$$

Thus, we can express (2) and (3) in a more compact way

$$V_{\text{C}} = \alpha_{\text{m}}^{-1} I_{\text{D}}^{1/m}(V_{\text{G}} - V_{\text{T}})^{-(1+\gamma)/m}, \qquad 1 \le m \le 2. \tag{12}$$

Although the range $1 \le m \le 2$ includes all the cases covered by (1), the practical cases can be restricted to the limit cases $m = 1$ and $m = 2$. The election of $m = 1$ or $m = 2$ is decided by a simple linear regression study of the $I_{\text{D}} - V_{\text{D}}$ curves at low values of V_{D}.

The combination of (7) and (12) defines a compact relation between the drain current and the external terminal voltages. This model has parameters that can be characterized relatively easily, or even guessed, preventing unnecessary phenomenological fitting parameters or even the use of transistors with different channel lengths. Our model is complemented with an extraction procedure of its parameters V_{T}, μ_{o}, γ, and α_{m} [or the equivalent $M(V_{\text{GS}})$ or $R_{\text{C}}(V_{\text{GS}}$] from the current–voltage curves of an OTFT. It follows the main ideas of the procedure proposed in [61] and [62]. However, some modifications are made in order to eliminate errors in the determination of the model parameters when large contact voltages are present and to extend its application to output characteristics measured in single-length transistors. As different models or different sets of values of our model can reproduce the experimental data, tests are also provided in order to validate the physical meaning of the extracted values for the parameters.

VI. Parameter Extraction Method

The objective of the extraction method is to determine the values of the parameters μ_{o}, γ, V_{T}, and α_{m} that define the compact model for the OTFT (7) including the contact effects (12). The independent determination of M (or R_{C}) for each V_{GS} is preferred to the determination of the compact parameter α_{m}. It is slower but more general, since it can be applied to situations where instabilities or trapping effects appear in the transistor [79]. In these cases, the evolution of σ_{channel} with V_{G} (9) can separate from a straight line due to slight modifications in the threshold voltage.

We propose a five step procedure with several tests to check the physical meaning of the results. In a previous work [74], we proposed a method to extract the parameters of this model from experimental $(I_{\text{D}} - V_{\text{D}})$ curves including the voltage drop at the contact. It was applied and tested successfully in an hypothetical p-type OTFT with known parameters [80]. It was adapted later to I_{D}–V_{D} curves with hysteresis [81]. In this paper, we compile all the previous ideas to make the method completely general and applicable to OTFTs.

A. Importance of a Compact Model With Contact Effects

Prior to the presentation of our characterization procedure, we highlight the importance of using a proper compact model for OTFTs with contact effects in the determination of essential device parameters such as the mobility μ and the threshold voltage V_{T}. It is deduced from many of the references cited in this paper that the apparent mobility extracted from current-voltage curves with contact effects is different from the real one. However, in many publications, the classical MOS model is still used to characterize the mobility. In saturation, the effects of the contacts are lower than in the linear region of operation. However, the saturation region is not free from errors. In the following, we determine such errors. To do this, we create a set of output characteristics for a hypothetical transistor for which we know all its parameters: $k_{\text{o}} = \mu_{\text{o}}C_{\text{i}}w/L$, γ, V_{T}, and M (or R_{C}). We build the output characteristics of this transistor by combining an intrinsic transistor modeled with the ideal MOS model plus a contact region at the source [Fig. 2(d)]. The classical MOS model can be easily deduced from (7) by assuming $V_{\text{S}} = 0$ V and $\gamma = 0$. The contact region is modeled by (2) or (3).

Once the output characteristics are created, the ideal MOS equations are used to extract the parameters of such a hypothetical transistor. Fig. 3 represents the errors in this determination in the saturation region. The test is done for different values of k, M, and R_{C} (M and R_{C} are assumed independent of the gate voltage; a dependence with the gate voltage would increase the error). Fig. 3 defines the ranges of these parameters where the relative error is not negligible and the classical MOS model is inaccurate. This figure is also useful since we can establish a relation between the values of M and R_{C} that produce the same effects.

B. Our Extraction Method

The five steps of our extraction procedure are (Fig. 4) now presented.

1) Initial estimation of μ and V_{T}. The experimental data in the saturation region are fitted with the classical MOS model [(7) with $\gamma = 0$ and $V_{\text{S}} = 0$ V] to determine apparent values for the threshold voltage and the mobility.
2) Initial estimation of M (or R_{C}). The contact model is added to the drain voltage by combining $V_{\text{D}} = V_{\text{DS}} + V_{\text{S}}$ and (3) [or (2)] and assuming $V_{\text{G}} = V_{\text{GS}}$

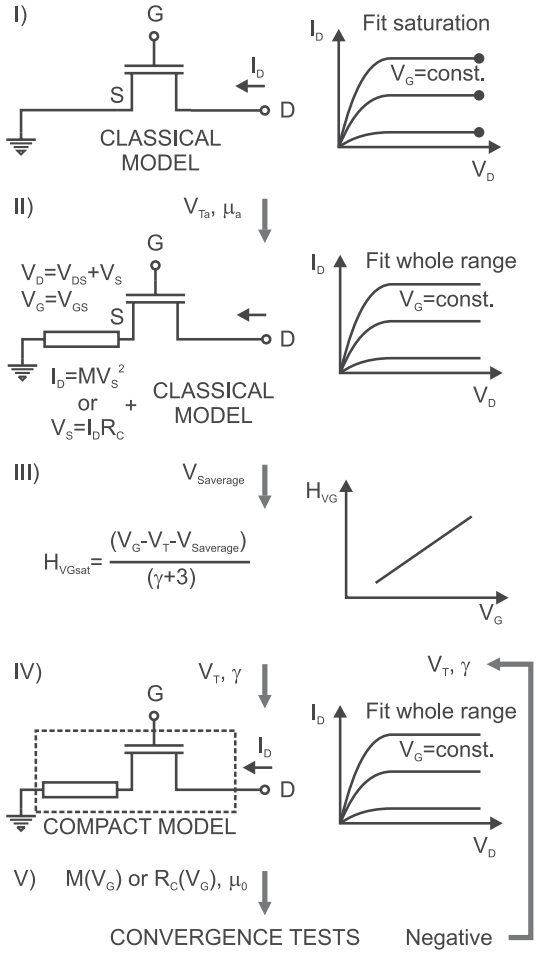

Fig. 4. Steps of the parameter extraction method indicating the models used (left) to analyze the experimental data (right).

[Fig. 4 II)]. The resulting equations are used to fit the whole experimental $I_D(V_D, V_G)$ curves to extract values of $M(V_G)$ (or $R_C(V_G)$). Then, an averaged value for the contact voltage in saturation, $V_{C_{\text{average}}}$, can be obtained.

3) Extraction of V_T and γ with the H_{VG} function [61], [82] applied to the experimental data in saturation. The H_{VG} function is defined as

$$H_{VG}(V_G) = \frac{\int_{<V_T}^{V_G} I_D dV_G}{I_D(V_G)}. \quad (13)$$

The H_{VG} function can be derived from the TFT generic model (7) in the linear and saturation modes. In the saturation mode ($V_D > (V_G - V_T)$), H_{VG} is linear with V_G [61]

$$H_{VG}(V_G) = \frac{(V_G - V_T - V_S)}{(\gamma + 3)}. \quad (14)$$

The values of γ and the threshold voltage V_T can be extracted easily from the slope of $H_{VG}(V_G)$ and intercept with the V_G axis, by assuming $V_S = V_{C_{\text{average}}}$ in (14).

4) Extraction of μ_o and M or R_C (or α_m). Assuming the previous values of V_T and γ as correct, the parameters μ_o and M are iteratively modified until a good fitting is obtained between the theoretical model (7) and (3) [or (2)] and the experimental data. As initial guessed values for the parameters μ_o and M, the ones obtained in steps 1) and 2), respectively, can be used. Since the experimental data are reproduced with a model that depends on several parameters different solutions may be expected. Thus, some tests must be done to validate the solution.

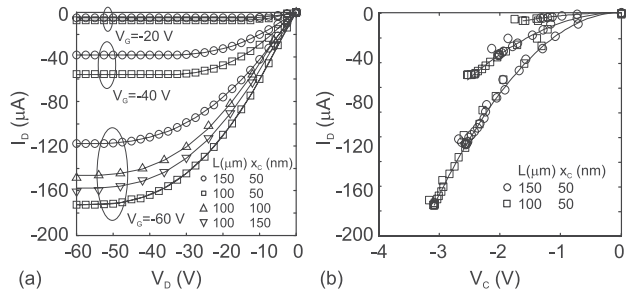

Fig. 5. (a) Comparison of output characteristics measured in pentacene-based OTFTs with Au S/D contacts (symbols) [83] and our numerical results (solid lines). Transistors with different channel length L and organic thickness x_C are studied. (b) I_D–V_C curves extracted by inserting in (7) the experimental data of (a) and the fitting values $V_T = -3.14$ V, $\gamma = 0.59$, and $\mu_o = 0.09$ cm^2/V$^{1+\gamma}$s (symbols); and by using (3) and (11) with $\alpha_2 = 3.9 \times 10^{-8}$ A/V$^{3+\gamma}$ (solid lines).

5) Tests of the solution.
   a) The values of the parameters (μ_o, γ and V_T) and the experimental data are introduced in the compact model (7). The I_D–V_C curves at the contact are extracted, and must be consistent with the trends expected by (3) [or (2)]. In case of a negative test, new values of γ and V_T must be proposed in part 4).
   b) Parameters M (or $1/R_C$) are represented as a function of V_G. These parameters include information about the free charge density at the contact region. Assuming that the free charge density in the channel and contact appears at the same voltage, the evolution of M (or $1/R_C$ with V_G) must intercept the V_G-axis at the value obtained for V_T. In case of a negative test, a new value of V_T must be proposed in part 4).

VII. Results and Discussion

To check the validity and applicability of our compact model with contact effects, (7) and (12), and the extraction method, we analyzed published I_D–V_D experimental curves from pentacene-based OTFTs at different conditions. We analyzed the effects of temperature, contact length, material length, barrier height at the interface, TC and BC configurations, and linear or nonlinear behavior. We also show a situation in which the parameters R_C or $1/M$ do not follow the trend with V_G indicated in (11). This can be typical of OTFTs with trapping effects.

A. Effects of the Size of the Structure

Fig. 5(a) shows a comparison of experimental data (symbols) with the results of our model (solid lines). They correspond to inverted-staggered OTFTs with thermally evaporated pentacene and Au S/D contacts [83], two different

TABLE I
FITTING PARAMETERS USED WITH DIFFERENT MODELS TO REPRODUCE THE DATA OF FIG. 5

Model	Ideal	H_{VG} $(V_S = 0)$	H_{VG}	Compact
V_T (V)	-10.31	-0.79	-3.14	-3.14
γ	0	0.49	0.49	0.52
μ_o $(cm^2/V^{1+\gamma}s)$	0.65	-	-	0.09

channel lengths ($L = 100$ and 150 μm) and different thickness of the pentacene semiconductor or contact lengths ($x_C = 50$, 100 and 150 nm). The whole set of curves is reproduced with our model with the same set of parameters: $V_T = -3.14$ V, $\gamma = 0.59$, $\mu_o = 0.09$ cm^2/V$^{1+\gamma}$s, and $\alpha_2 = 3.9 \times 10^{-8} \times$ (50 nm/x_C) A/V$^{3+\gamma}$. A convergence test is made to validate these parameters [Fig. 5(b)]. Combining in (7) the above values of μ_o, γ, and V_T with the experimental values (I_D, V_D) corresponding to $x_C = 50$ nm of Fig. 5(a), then the current-voltage curves at the contact can be obtained [symbols in Fig. 5(b)]. In the same figure, the curves I_D–V_C calculated from (3) and (11) with $\alpha_2 = 3.9 \times 10^{-8}$ A/V$^{3+\gamma}$ are shown in solid lines. The matching of the symbols and solid lines indicates that the solution is physically acceptable. Table I shows the values of the parameters of the model extracted during the different steps of the fitting procedure. The value of the threshold voltage is modified in the different steps. This value depends on the model employed and whether contact effects are included or not. Actually, the value extracted from the H_{VG} is valid only when the averaged contact voltage ($V_S = V_{C_{\text{average}}}$) is considered in (14). The value of the mobility is also altered during the fitting procedure, from a constant value with the ideal MOS model to a gate-voltage dependent relation modeled by μ_o and γ. In the table, the value of the mobility obtained with the ideal MOS model is greater than the one obtained for μ_o with the compact model. The value of μ_o must be understood as the value of the mobility at $V_{GT} = 1$ V. The value at $V_{GT} = 40$ V is $\mu = 0.61$ cm^2/Vs. For these samples, the value obtained with the compact model represents an averaged value, since the averaged contact voltage is not too large $V_{C_{\text{average}}} \approx -2.4$ V.

The value of μ_o is in agreement with the value reported in [83] for the mobility in the conducting channel, in the range of 0.3–0.5 cm^2/Vs. In [83], the path that the current follows from the TC down to the conducting channel is modeled with a factor about 3 lower mobility, attributed to an anisotropic mobility. The anisotropic conduction in the contact region and in the intrinsic channel is also compatible with our model. Assuming the same value for the mobility in the contact region and in the conducting channel and introducing the value extracted for α_2 and the geometrical parameters of the OTFTs [83] in (3) and (11), the free to total charge ratio θ is found to be greater than one. Thus, a lower value of the mobility is necessary to obtain values of θ with a physical meaning. A value around 10^{-4} cm^2/Vs, as provided in [83], results in values of θ in the range $[0.001, 0.0071]$ for gate voltages in the range $[-20, -60]$ V.

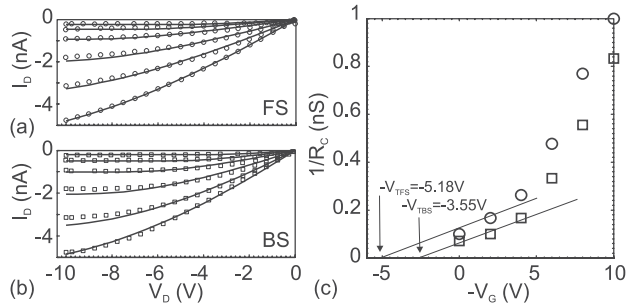

Fig. 6. (a) and (b) Comparison of experimental output characteristics of a top gate staggered PVA/pentacene/Au OFET [84], with our compact model (solid lines). $V_G = 0$ to -10 V from top to bottom with a -2 V step (FS, circles; and BS, squares). (c) Extracted values of $1/R_C$ in the FS (circles) and BS (squares). The extrapolation of the data at low gate voltages intercept with the V_G-axis at points close to $V_{T_{FS}} = 5.18$ V and $V_{T_{BS}} = 3.55$ V.

B. Transistor with Instabilities

Fig. 6(a) and (b) shows, with symbols, the output characteristics with hysteresis measured in a top gate staggered pentacene OFET with Au S/D electrodes [84]. The gate dielectric is Poly(vinyl alcohol) (PVA), known to produce hysteresis in OTFTs. The dielectric thickness is $t_i = 1$ μm, the channel length $L = 100$ μm, the transistor width $w = 1$ mm and the organic-film thickness $t_o = 100$ nm. These current-voltage curves in the forward scan (FS) and the backward scan (BS) are compared with the compact model (7) in combination with the linear model (2). Our numerical results are shown in solid lines in Fig. 6(a) and (b). The parameters obtained from the fitting procedure are: $\mu_o = 0.0041$ cm^2/(V$^{1+\gamma}$s), $k_0 = 1.4 \times 10^{-10}$ A/V$^{2+\gamma}$, $\gamma = 0.05$, $V_{T_{FS}} = 5.18$ V, and $V_{T_{BS}} = 3.55$ V. The values of $1/R_C$ in (2) are represented as a function of V_G for the FS and BS in Fig. 6(c). Since the charge density in the contact is proportional to $1/R_C$, this figure shows how the threshold voltages of the charge density in (4) coincide with the values of $V_{T_{FS}}$ and $V_{T_{BS}}$ found in the fitting procedure. Thus, the values of the fitting parameters are coherent among themselves and the solution can be considered physically acceptable.

At higher voltages, the evolution of the charge density at the contact deviates from the linear trend. The free charge density usually follows a linear trend with the gate voltage (9). However, in situations where instabilities or trapping effects appear in the transistor, the threshold voltage can vary and σ_{channel} can deviate from this trend. In cases of slight modifications of the threshold voltage, our model is still valid [81]. Instead of combining (7) and (12), (7) must be combined with (2) or (3). In these cases, the independent determination of M or R_C for each V_{GS} is preferred to the determination of the compact parameter α_m. We have reported how information of the trapping processes during hysteresis can be extracted with the analysis of the contact region of the transistor [81].

C. Effects of the Temperature

In Fig. 7, we analyzed experimental data measured at different temperatures on bottom gate evaporated-pentacene based OFETs with top Au S/D contacts, $L = 100$ μm and $w = 700$ μm [58]. The thickness of the SiO_2 is 270 nm and the

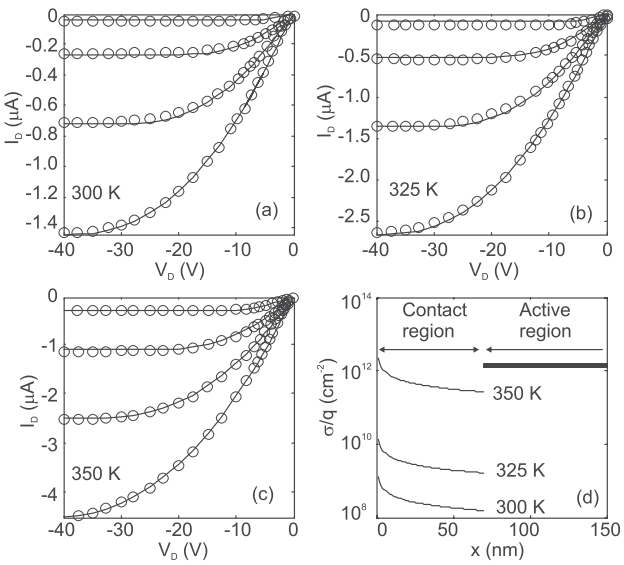

Fig. 7. (a)–(c) Comparison of experimental output characteristics taken at different temperatures of a bottom gate pentacene based OFET with Au TCs [58] (symbols), with our compact model (solid lines). $V_G = -10$, -20, -30, and -40 V from top to bottom. (d) Surface concentration of free charges along the channel of the OTFT at different temperatures for $V_G = -20$ V.

TABLE II
FITTING PARAMETERS USED TO REPRODUCE THE EXPERIMENTAL DATA OF FIG. 7

T (K)	V_T (V)	γ	k_0 (A/V$^{2+\gamma}$)	μ_o (cm^2/V$^{1+\gamma}$s)	α_2 (A/V$^{3+\gamma}$)
300	0.3	0.49	3.4×10^{-10}	0.005	2.4×10^{-9}
325	0.44	0.3	1.3×10^{-9}	0.015	10^{-7}
350	2	0.14	3.4×10^{-9}	0.042	5.0×10^{-6}

pentacene thickness, which is the same as contact length x_C, is 70 nm. The experimental curves have been reproduced with our model with the parameters shown in Table II. On the one side, the variation of the threshold voltage with temperature can be considered large. This variation can be attributed to propagation of errors in the determination of the contact voltage. In any case, the result improves the much greater variation obtained in [58]. Studies focusing on OTFTs without contact effects obtain an even lower variation of the threshold voltage [85]. On the other side, the parameter γ follows the trend with the temperature given in (8) with $T_o = 373.8$ K, and μ_o also follows the trend with temperature proposed in [64, eq. (15)] with $\sigma_0 = 10^8$ S/cm and $\alpha^{-1} = 0.31$ Å, thus validating our results.

The average contact voltage is estimated from these parameters, resulting in $V_{C_{\text{average}}} = -1.8$, -0.4, -0.1 V at 300, 325, and 350 K, respectively. The contact effects decrease when the temperature increases. Another way to analyze the effects of the contacts with the temperature is by evaluating the surface free-charge density at the contact region. Assuming $V_{C_0} = -1$ V in (6), the surface concentration of free charges at the contact can be compared with the surface concentration of free charges along the channel. Fig. 7(d) shows this comparison evaluated at $V_G = -20$ V. At 350 K the effect of the contact region is almost negligible since the free charge density is almost uniform along the whole structure. However, at 300 K, the free charge density in the contact region is almost four orders of magnitude lower than in the channel.

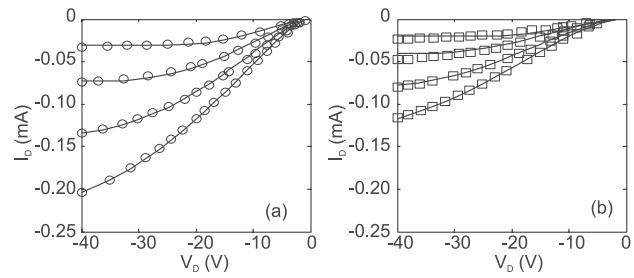

Fig. 8. Comparison of experimental output characteristics measured in a BC pentacene based OFET with Au-Pd contacts [2] (symbols), with our compact model (solid lines). $V_G = -10$, -20, -30, and -40 V from top to bottom. (a) Au source/Pd drain. (b) Pd source/Au drain.

D. Effects of the Energy Barrier

In Fig. 8, we analyzed the experimental data measured in a BC pentacene TFT with Au-Pd contacts [2]. The dimensions of the transistor are $L = 10$ μm, $w = 220$ μm, and the gate dielectric is SiO_2 with 290-nm thickness. Fig. 8(a) corresponds to the configuration Au-source/Pd-drain, and Fig. 8(b), to the configuration Pd-source/Au-drain. The solid lines in both figures show the results of our model using the parameters: $V_T = 16$ V, $\gamma = 0.18$, and $\mu_o = 0.47$ cm^2/V$^{1+\gamma}$s, ($k_o = 5.02 \times 10^{-8}$ A/V$^{2+\gamma}$). The effect of changing the electrode only affects the value of the parameter α_2: $\alpha_2(\text{Au}) = 2.61 \times 10^{-9}\text{A/V}^{3+\gamma}$ and $\alpha_2(\text{Pd}) = \alpha_2(\text{Au})/5.19 = 5.04 \times 10^{-10}\text{A/V}^{3+\gamma}$. However, the use of the classical MOS model to characterize the transistor in Fig. 8 gives different values for the mobility and the threshold voltage: $\mu = 0.63$ and 0.42 cm^2/Vs and $V_T = 15$ and 14 V for Fig. 8(a) and (b), respectively [2]. The importance of using a proper compact model that includes the contact effects of OTFTs is again demonstrated. On average the voltage drop at the contacts is $V_{C\text{average}} = -9.64$ V.

VIII. IDEAS FOR FUTURE WORK

One of the strengths of our model is the capability to separate the charge density at the contact region from the charge density in the channel. We have seen that changes in the temperature lead to small changes in the free charge density in the channel but large changes in the contact region [Fig. 7(d)]. Some of the niche applications where OTFTs play an important role are as sensors [86], [87] or photodetectors [88], for example. Monitoring the free charge density in the contact region under the presence of different atmospheres or irradiation might help to explain the sensing characteristics of these devices. In this regard, our model is a potential tool for this task.

In fact, these suggestions agree with recent studies of chemical sensors [87] and phototransistors. [88]. The generation of charges by different physical or chemical mechanisms and

the trap charging in the contact regions decrease the contact resistance. The chemical or irradiation effects on the TFT parameters such as the off-current, threshold voltage, bulk mobility, and field-effect mobility can be investigated using our model. A link between the contact resistance and the threshold voltage would open the possibility of designing the source and drain contacts using different metals or incorporating SAMs to optimize R_C and maximize the sensing effect in organic TFTs.

Another strength of our model is its applicability to OTFTs that differ in structure and morphology. The parameter α_m added to the generic drift MOS model is enough to quantify the effects of the contacts. One step forward in the improvement of OTFTs would be to find the relation between this parameter and structural variations in the active organic material, such as grain boundaries, interface states or defects. This would help to achieve good reproducibility in the fabrication of OTFTs. We have seen in this paper an example of what is found in the state-of-the-art OTFTs: a great variability in the characteristics of similar OTFTs. Until the technology achieves good reproducibility in the fabrication of OTFTs, simple and tunable compact models such as the one presented in this paper must run in parallel with high accuracy measurements [71], [72].

IX. Conclusion

By carefully inspecting past and current achievements in modeling the contact effects of OTFTs, we have proposed a model for the current–voltage curves at the contact region that unifies different trends found in experimental data. This model, which is characterized by only one parameter, has been embedded in a generic charge drift model that also includes a gate voltage-dependent mobility. The model is easily reduced to the generic FET model with a constant mobility and no contact effects.

We have proposed a characterization procedure to extract the values of the parameters of the OTFT model, which does not need major reassessment as compared to those for crystalline FETs. We have obtained reliable and good fitting of the TFT generic model to experimental data. We have checked the consistency in the bridge between physical origin of the contact effects and the parameters of the model. The proposed model is a powerful tool to describe the large amount of different structures or fabrication processes the same type organic material in an OTFT can be subjected to. The model captures, in a consistent and relatively simple way, the essential behavior of transistors when temperature, channel length, and width and different energy barriers at the contact region are varied. It also provides information about the free charge density along the transistor channel.

References

[1] O. Marinov, M. J. Deen, and B. Iñiguez, "Charge transport in organic and polymer thin-film transistors: Recent issues," *IEE Proc., Circuits, Devices Syst.*, vol. 152, no. 3, pp. 189–209, Jun. 2005.

[2] D. J. Gundlach, L. Zhou, J. A. Nichols, T. N. Jackson, P. V. Necliudov, and M. S. Shur, "An experimental study of contact effects in organic thin film transistors," *J. Appl. Phys.*, vol. 100, no. 2, pp. 024509-1–024509-13, 2006.

[3] C. H. Kim, Y. Bonnassieux, and G. Horowitz, "Charge distribution and contact resistance model for coplanar organic field-effect transistors," *IEEE Trans. Electron Devices*, vol. 60, no. 1, pp. 280–287, Jan. 2013.

[4] A. H. Castro Neto, F. Guinea, N. M. R. Peres, K. S. Novoselov, and A. K. Geim, "The electronic properties of graphene," *Rev. Mod. Phys.*, vol. 81, no. 1, pp. 109–162, Jan./Mar. 2009.

[5] I. Popov, G. Seifert, and D. Tomanek, "Designing electrical contacts to MoS_2 monolayers: A computational study," *Phys. Rev. Lett.*, vol. 108, no. 15, pp. 156802-1–156802-5, Apr. 2012.

[6] H. K. Seong, E. K. Jeon, M. H. Kim, H. Oh, J. O. Lee, J. J. Kim, and H. J. Choi, "Interface charge induced p-type characteristics of aligned $Si_{1-x}Ge_x$ nanowires," *Nano Lett.*, vol. 8, no. 11, pp. 3656–3661, Nov. 2008.

[7] B. Ma, B. J. Kim, L. Deng, D. A. Poulsen, M. E. Thompson, and J. M. J. Fréchet, "Bipolar copolymers as host for electroluminescent devices: Effects of molecular structure on film morphology and device performance," *Macromolecules*, vol. 40, no. 23, pp. 8156–8161, 2007.

[8] S. Chung, J. Jeong, D. Kim, Y. Park, C. Lee, and Y. Hong, "Contact resistance of inkjet-printed silver source–drain electrodes in bottom-contact OTFTs," *J. Display Technol.*, vol. 8, no. 1, pp. 48–53, 2012.

[9] J. J. Kim, M. K. Han, and Y. Y. Noh, "Flexible OLEDs and organic electronics," *Semicond. Sci. Technol.*, vol. 26, no. 3, p. 030301, 2011.

[10] K. Nagashio and A. Toriumi, "Density-of-states limited contact resistance in graphene field-effect transistors," *Jpn. J. Appl. Phys.*, vol. 50, no. 7, pp. 070108-1–070108-6, Jul. 2011.

[11] S. M. Sze, *Physics of Semiconductor Devices*. New York, NY, USA: Wiley, 1981.

[12] M. J. Deen and P. K. Basu, *Silicon Photonics. Fundamentals and Devices*. New York, NY, USA: Wiley, 2012.

[13] N. Mott, "Note on the contact between a metal and an insulator or semiconductor," *Proc. Cambridge Phil. Soc.*, vol. 34, no. 4, pp. 568–572, 1938.

[14] W. Schottky, "Discrepencies in Ohm's laws in semiconductors," *Phys. Zeits.*, vol. 41, pp. 570–573, 1940.

[15] F. Xia, V. Perebeinos, Y. M. Lin, Y. Wu, and P. Avouris, "The origins and limits of metal-graphene junction resistance," *Nature Nanotechnol.*, vol. 6, no. 3, pp. 179–184, Mar. 2011.

[16] T. Wang, B. Yu, Y. Liu, and M. J. Deen, "Investigation of electrically induced migration of copper on grapheme surfaces: Theory and experiments," *Appl. Phys. Lett.*, vol. 103, no. 7, pp. 073104-1–073104-3, 2013.

[17] S. M. Song, J. K. Park, O. J. Sul, and B. J. Cho, "Determination of work function of graphene under a metal electrode and its role in contact resistance," *Nano Lett.*, vol. 12, no. 8, pp. 3887–3892, Aug. 2012.

[18] G. Giovannetti, P. A. Khomyakov, G. Brocks, V. M. Karpan, J. van den Brink, and P. J. Kelly, "Doping graphene with metal contacts," *Phys. Rev. Lett.*, vol. 101, no. 2, pp. 026803-1–026803-4, Jul. 2008.

[19] R. T. Tung, "Chemical bonding and Fermi level pinning at metal-semiconductor interfaces," *Phys. Rev. Lett.*, vol. 84, no. 26, pp. 6078–6081, Jun. 2000.

[20] V. Heine, "Theory of surface states," *Phys. Rev.*, vol. 138, no. 6A, pp. 1689–1696, 1965.

[21] J. Tersoff, "Schottky-barrier heights and the continuum of gap states," *Phys. Rev. Lett.*, vol. 52, no. 6, pp. 465–468, 1984.

[22] Y. He, J. Zhang, S. Hou, Y. Wang, and Z. Yu, "Schottky barrier formation at metal electrodes and semiconducting carbon nanotubes," *Appl. Phys. Lett.*, vol. 94, no. 9, pp. 093107-1–093107-3, 2009.

[23] S. Braun, W. R. Salaneck, and M. Fahlman, "Energy-level alignment at organic/metal and organic/organic interfaces," *Adv. Mater.*, vol. 21, nos. 14–15, pp. 1450–1472, 2009.

[24] Z. Liu, M. Kobayashi, B. C. Paul, Z. Bao, and Y. Nishi, "Contact engineering for organic semiconductor devices via Fermi level depinning at the metal-organic interface," *Phys. Rev. B*, vol. 82, pp. 035311-1–035311-6, Jul. 2010.

[25] S. Yadav, P. Kumar, and S. Ghosh, "Optimization of surface morphology to reduce the effect of grain boundaries and contact resistance in small molecule based thin film transistors," *Appl. Phys. Lett.*, vol. 101, no. 19, pp. 193307-1–193307-4, 2012.

[26] J. H. Seo, A. Gutacker, B. Walker, S. Cho, A. Garcia, R. Yang, T. Q. Nguyen, A. J. Heeger, and G. C. Bazan, "Improved injection in n-type organic transistors with conjugated polyelectrolytes," *J. Amer. Chem. Soc.*, vol. 131, no. 51, pp. 18220–18221, 2009.

[27] D. Braga, M. Ha, W. Xie, and C. D. Frisbie, "Ultralow contact resistance in electrolyte-gated organic thin film transistors," *Appl. Phys. Lett.*, vol. 97, no. 19, pp. 193311-1–193311-3, 2010.

[28] J. Knoch, Z. Chen, and J. Appenzeller, "Properties of metal-graphene contacts," *IEEE Trans. Nanotechnol.*, vol. 11, no. 3, pp. 513–519, May 2012.

[29] L. Yan, C. Punckt, I. A. Aksay, W. Mertin, and G. Bacher, "Local voltage drop in a single functionalized graphene sheet characterized by Kelvin probe force microscopy," *Nano Lett.*, vol. 11, no. 9, pp. 3543–3549, Sep. 2011.

[30] Y. Khatami, H. Li, C. Xu, and K. Banerjee, "Metal-to-multilayer-graphene contact—Part I: Contact resistance modeling," *IEEE Trans. Electron Devices*, vol. 59, no. 9, pp. 2444–2452, Sep. 2012.

[31] S. Das, H. Y. Chen, A. V. Penumatcha, and J. Appenzeller, "High performance multilayer MoS_2 transistors with scandium contacts," *Nano Lett.*, vol. 13, no. 1, pp. 100–105, Jan. 2013.

[32] H. Qiu, L. Pan, Z. Yao, J. Li, Y. Shi, and X. Wang, "Electrical characterization of back-gated bi-layer MoS_2 field-effect transistors and the effect of ambient on their performances," *Appl. Phys. Lett.*, vol. 100, no. 12, pp. 123104-1–123104-3, Mar. 2012.

[33] B. Liu, Y. Wang, S. Dilts, T. S. Mayer, and S. E. Mohney, "Silicidation of silicon nanowires by platinum," *Nano Lett.*, vol. 7, no. 3, pp. 818–824, Mar. 2007.

[34] I. Kymissis, C. Dimitrakopoulos, and S. Purushothaman, "High-performance bottom electrode organic thin-film transistors," *IEEE Trans. Electron Devices*, vol. 48, no. 6, pp. 1060–1064, Jun. 2001.

[35] S. Scheinert and G. Paasch, "Fabrication and analysis of polymer field effect transistors," *Phys. Stat. Sol. A*, vol. 201, no. 6, pp. 1263–1301, 2004.

[36] S. D. Wang, Y. Yan, and K. Tsukagoshi, "Understanding contact behavior in organic thin film transistors," *Appl. Phys. Lett.*, vol. 97, no. 6, pp. 063307-1–063307-3, 2010.

[37] H. Wang, L. Li, Z. Ji, C. Lu, J. Guo, L. Wang, and M. Liu, "Contact-length-dependent contact resistance of top-gate staggered organic thin-film transistors," *IEEE Electron Device Lett.*, vol. 34, no. 1, pp. 69–71, Jan. 2013.

[38] M. J. Deen and F. Pascal, "Electrical characterization of semiconductor materials and devices—Review," *J. Mater. Sci., Mater. Electron.*, vol. 17, no. 8, pp. 549–575, Aug. 2006.

[39] G. Reeves and H. Harrison, "Obtaining the specific contact resistance from transmission-line model measurements," *Electron Device Lett.*, vol. 3, no. 5, pp. 111–113, 1982.

[40] R. Nouchi, T. Saito, and K. Tanigaki, "Observation of negative contact resistances in graphene field-effect transistors," *J. Appl. Phys.*, vol. 111, no. 8, pp. 084314-1–084314-7, Apr. 2012.

[41] R. Nouchi and K. Tanigaki, "Empirical modeling of metal-contact effects on graphene field-effect transistors," *Jpn. J. Appl. Phys.*, vol. 50, no. 7, pp. 070109-1–070109-4, Jul. 2011.

[42] S. E. Mohney, Y. Wang, M. A. Cabassi, K. K. Lew, S. Dey, J. M. Redwing, and T. S. Mayer, "Measuring the specific contact resistance of contacts to semiconductor nanowires," *Solid-State Electron.*, vol. 49, no. 2, pp. 227–232, Feb. 2005.

[43] H. Park, R. Beresford, R. Ha, H. J. Choi, H. Shin, and J. Xu, "Evaluation of metal-nanowire electrical contacts by measuring contact end resistance," *Nanotechnology*, vol. 23, no. 24, pp. 245201-1–245201-7, Jun. 2012.

[44] J. Hu, Y. Liu, C. Z. Ning, R. Dutton, and S. M. Kang, "Fringing field effects on electrical resistivity of semiconductor nanowire-metal contacts," *Appl. Phys. Lett.*, vol. 92, no. 8, pp. 083503-1–083503-3, Feb. 2008.

[45] T. Mueller, F. Xia, M. Freitag, J. Tsang, and P. Avouris, "Role of contacts in graphene transistors: A scanning photocurrent study," *Phys. Rev. B*, vol. 79, no. 24, pp. 245430-1–245430-6, Jun. 2009.

[46] F. Leonard and A. A. Talin, "Electrical contacts to one- and two-dimensional nanomaterials," *Nature Nanotechnol.*, vol. 6, no. 12, pp. 773–783, Dec. 2011.

[47] F. Xia, T. Mueller, R. Golizadeh-Mojarad, M. Freitag, Y.-M. Lin, J. Tsang, and V. Perebeinos, P. Avouris, "Photocurrent imaging and efficient photon detection in a graphene transistor," *Nano Lett.*, vol. 9, no. 3, pp. 1039–1044, Mar. 2009.

[48] L. Bürgi, T. J. Richards, R. H. Friend, and H. Sirringhaus, "Close look at charge carrier injection in polymer field-effect transistors," *J. Appl. Phys.*, vol. 94, no. 9, pp. 6129–6137, 2003.

[49] M. Estrada, I. Mejía, A. Cerdeira, J. Pallares, L. F. Marsal, and B. Iñiguez, "Mobility model for compact device modeling of OTFTs made with different materials," *Solid-State Electron.*, vol. 52, no. 5, pp. 787–794, 2008.

[50] N. F. Mott and R. W. Gurney, *Electronic Processes in Ionic Crystals*. New York, NY, USA: Oxford Univ. Press, 1940.

[51] P. V. Necliudov, M. S. Shur, D. J. Gundlach, and T. N. Jackson, "Modeling of organic thin film transistors of different designs," *J. Appl. Phys.*, vol. 88, no. 11, pp. 6594–6597, 2000.

[52] S. D. Wang, T. Minari, T. Miyadera, K. Tsukagoshi, and Y. Aoyagi, "Contact-metal dependent current injection in pentacene thin-film transistors," *Appl. Phys. Lett.*, vol. 91, no. 20, pp. 203508-1–203508-3, 2007.

[53] A. Valletta, A. Daami, M. Benwadih, R. Coppard, G. Fortunato, M. Rapisarda, F. Torricelli, and L. Mariucci, "Contact effects in high performance fully printed p-channel organic thin film transistors," *Appl. Phys. Lett.*, vol. 99, no. 23, pp. 233309-1–233309-4, 2011.

[54] M. J. Deen, M. H. Kazemeini, and S. Holdcroft, "Contact effects and extraction of intrinsic parameters in poly(3-alkylthiophene) thin film field-effect transistors," *J. Appl. Phys.*, vol. 103, no. 12, pp. 124509-1–124509-7, 2008.

[55] P. Lara Bullejos, J. A. Jiménez Tejada, S. Rodríguez-Bolívar, M. J. Deen, and O. Marinov, "Model for the injection of charge through the contacts of organic transistors," *J. Appl. Phys.*, vol. 105, no. 8, pp. 084516-1–084516-8, 2009.

[56] V. Vinciguerra, M. L. Rosa, D. Nicolosi, G. Sicurella, and L. Occhipinti, "Modeling the gate bias dependence of contact resistance in staggered polycrystalline organic thin film transistors," *Org. Electron.*, vol. 10, no. 6, pp. 1074–1081, 2009.

[57] Y. Hong, F. Yan, P. Migliorato, S. Han, and J. Jang, "Injection-limited contact in bottom-contact pentacene organic thin-film transistors," *Thin Solid Films*, vol. 515, nos. 7–8, pp. 4032–4035, 2007.

[58] Y. J. Lin and B. C. Huang, "Influence of the contact resistance effect on the output characteristics of pentacene-based organic thin film transistors," *Microelectron. Eng.*, vol. 103, pp. 76–78, Mar. 2013.

[59] T. B. Singh, N. Marjanović, G. J. Matt, N. S. Sariciftci, R. Schwödiauer, and S. Bauer, "Nonvolatile organic field-effect transistor memory element with a polymeric gate electret," *Appl. Phys. Lett.*, vol. 85, no. 22, pp. 5409–5411, 2004.

[60] M. Estrada, A. Cerdeira, J. Puigdollers, L. Reséndiz, J. Pallares, L. F. Marsal, C. Voz, and B. Iñiguez, "Accurate modeling and parameter extraction method for organic TFTs," *Solid-State Electron.*, vol. 49, no. 6, pp. 1009–1016, 2005.

[61] O. Marinov, M. J. Deen, U. Zschieschang, and H. Klauk, "Organic thin-film transistors: Part I—Compact DC modeling," *IEEE Trans. Electron Devices*, vol. 56, no. 12, pp. 2952–2961, Dec. 2009.

[62] M. J. Deen, O. Marinov, U. Zschieschang, and H. Klauk, "Organic thin-film transistors: Part II—Parameter extraction," *IEEE Trans. Electron Devices*, vol. 56, no. 12, pp. 2962–2968, Dec. 2009.

[63] M. Shur and M. Hack, "Physics of amorphous silicon based alloy field-effect transistors," *J. Appl. Phys.*, vol. 55, no. 10, pp. 3831–3842, 1984.

[64] M. C. J. M. Vissenberg and M. Matters, "Theory of the field-effect mobility in amorphous organic transistors," *Phys. Rev. B*, vol. 57, no. 20, pp. 12964–12967, May 1998.

[65] E. Calvetti, A. Savio, Z. M. Kovács-Vajna, and L. Colalongo, "Analytical model for organic thin-film transistors operating in the subthreshold region," *Appl. Phys. Lett.*, vol. 87, no. 22, pp. 223506-1–223506-3, 2005.

[66] L. Mariucci, M. Rapisarda, A. Valletta, S. Jacob, M. Benwadih, and G. Fortunato, "Current spreading effects in fully printed p-channel organic thin film transistors with Schottky source and drain contacts," *Org. Electron.*, vol. 14, no. 1, pp. 86–93, 2013.

[67] M. Rapisarda, A. Valletta, A. Daami, S. Jacob, M. Benwadih, R. Coppard, G. Fortunato, and L. Mariucci, "Analysis of contact effects in fully printed p-channel organic thin film transistors," *Org. Electron.*, vol. 13, no. 10, pp. 2017–2027, 2012.

[68] P. Lara Bullejos, J. A. Jiménez Tejada, M. J. Deen, O. Marinov, and W. R. Datars, "Unified model for the injection and transport of charge in organic diodes," *J. Appl. Phys.*, vol. 103, no. 6, pp. 064504-1–064504-12, 2008.

[69] P. Lara Bullejos, J. A. Jiménez Tejada, F. M. Gómez-Campos, M. J. Deen, and O. Marinov, "Evaluation of the charge density in the contact region of organic thin film transistors," *J. Appl. Phys.*, vol. 106, no. 9, pp. 094503-1–094503-4, 2009.

[70] A. Raychaudhuri, J. Kolk, M. J. Deen, and M. I. H. King, "A simple method to extract the asymmetry in parasitic source and drain resistances from measurements on a MOS transistor," *IEEE Trans. Electron Devices*, vol. 42, no. 7, pp. 1388–1390, Jul. 1995.

[71] L. S. C. Pingree, O. G. Reid, and D. S. Ginger, "Electrical scanning probe microscopy on active organic electronic devices," *Adv. Mater.*, vol. 21, no. 1, pp. 19–28, 2009.

[72] L. C. Teague, O. D. Jurchescu, C. A. Richter, S. Subramanian, J. E. Anthony, T. N. Jackson, D. J. Gundlach, and J. G. Kushmerick, "Probing stress effects in single crystal organic transistors by scanning Kelvin probe microscopy," *Appl. Phys. Lett.*, vol. 96, no. 20, pp. 203305-1–203305-3, 2010.

[73] A. K. Agarwal and B. Mazhari, "Simultaneous extraction of source and drain resistances in top contact organic thin film transistors from a single test structure," *Org. Electron.*, vol. 13, no. 11, pp. 2659–2666, 2012.

[74] J. A. Jiménez Tejada, K. M. Awawdeh, J. A. López Villanueva, J. E. Carceller, M. J. Deen, N. B. Chaure, T. Basova, and A. K. Ray, "Contact effects in compact models of organic thin film transistors: Application to zinc phthalocyanine-based transistors," *Org. Electron.*, vol. 12, no. 5, pp. 832–842, 2011.

[75] O. Marinov, M. J. Deen, and R. Datars, "Compact modeling of charge carrier mobility in organic thin-film transistors," *J. Appl. Phys.*, vol. 106, no. 6, pp. 064501-1–064501-13, 2009.

[76] S. D. Wang, T. Minari, T. Miyadera, K. Tsukagoshi, and J. X. Tang, "Contact resistance instability in pentacene thin film transistors induced by ambient gases," *Appl. Phys. Lett.*, vol. 94, no. 8, pp. 083309-1–083309-3, 2009.

[77] Y. Ishikawa, Y. Wada, and T. Toyabe, "Origin of characteristics differences between top and bottom contact organic thin film transistors," *J. Appl. Phys.*, vol. 107, no. 5, pp. 053709-1–053709-7, 2010.

[78] B. G. Streetman, *Solid State Electronic Devices*. Englewood Cliffs, NJ, USA: Prentice-Hall, 1980.

[79] O. Marinov, M. J. Deen, J. Yu, G. Vamvounis, S. Holdcroft, and W. Woods, "Variable current transport in polymer thin film transistors," *J. Vac. Sci. Technol. A*, vol. 22, no. 3, pp. 755–759, 2004.

[80] K. M. Awawdeh, J. A. Jiménez Tejada, J. A. López Villanueva, J. E. Carceller, M. J. Deen, N. B. Chaure, T. Basova, and A. K. Ray, "Compact modeling of the contact effects in organic thin film transistors," in *Proc. Spanish Conf. Electron Devices*, Feb. 2011, pp. 1–4.

[81] K. M. Awawdeh, J. A. Jiménez Tejada, P. López Varo, J. A. López Villanueva, and M. J. Deen, "Influence of the contact effects on the variation of the trapped charge in the intrinsic channel of organic thin film transistors," in *Proc. Spanish Conf. Electron Devices*, 2013, pp. 71–74.

[82] A. Cerdeira, M. Estrada, R. García, A. Ortiz Conde, and F. García Sánchez, "New procedure for the extraction of basic a-Si:H TFT model parameters in the linear and saturation regions," *Solid-State Electron.*, vol. 45, no. 7, pp. 1077–1080, 2001.

[83] C. W. Sohn, T. U. Rim, G. B. Choi, and Y. H. Jeong, "Analysis of contact effects in inverted-staggered organic thin-film transistors based on anisotropic conduction," *IEEE Trans. Electron Devices*, vol. 57, no. 5, pp. 986–994, May 2010.

[84] M. Egginger, "Electrical characterisation of poly(vinyl alcohol) based organic field effect transistors," Ph.D. dissertation, Inst. für Physikalishe Chemie, Johannes Kepler Univ. Linz, Linz, Austria, 2009.

[85] M. Estrada, A. Cerdeira, I. Mejia, M. Avila, R. Picos, L. F. Marsal, J. Pallares, and B. Iñiguez, "Modeling the behavior of charge carrier mobility with temperature in thin-film polymeric transistors," *Microelectron. Eng.*, vol. 87, no. 12, pp. 2565–2570, 2010.

[86] D. A. Bernards, D. J. Macaya, M. Nikolou, J. A. DeFranco, S. Takamatsu, and G. G. Malliaras, "Enzymatic sensing with organic electrochemical transistors," *J. Mater. Chem.*, vol. 18, no. 1, pp. 116–120, 2008.

[87] L. Torsi, F. Marinelli, M. D. Angione, A. Dell'Aquila, N. Cioffi, E. De Giglio, and L. Sabbatini, "Contact effects in organic thin-film transistor sensors," *Org. Electron.*, vol. 10, no. 2, pp. 233–239, 2009.

[88] M. J. Deen and M. H. Kazemeini, "Photosensitive polymer thin-film FETs based on poly(3-octylthiophene)," *Proc. IEEE*, vol. 93, no. 7, pp. 1312–1320, Jul. 2005.

Juan Antonio Jiménez Tejada (M'90) received the Ph.D. degree from the University of Granada, Granada, Spain, in 1991.

He is currently a Professor with the University of Granada.

Juan Antonio López Villanueva (M'90–SM'01) received the Ph.D. degree from the University of Granada, Granada, Spain, in 1990.

He has been a Full Professor with the University of Granada since 2003.

Pilar López Varo (M'13) is currently pursuing the Ph.D. degree with Universidad de Granada, Granada, Spain.

Her current research interests include transport and the injection of charge in organic diodes and the characterization of organic transistors.

Karam M. Awawdeh received the M.Sc. and Ph.D. degrees in physics from the University of Granada, Granada, Spain, in 2010 and 2013, respectively.

He joined the Faculty of Science, University of Hebron, Hebron, Palestine, in 2001.

M. Jamal Deen (F'02) received the Ph.D. degree in electrical engineering and applied physics from Case Western Reserve University, Cleveland, OH, USA, in 1985.

He is currently a Professor of electrical and computer engineering, McMaster University, Hamilton, ON, Canada.